PALEOCEANOGRAPHY, VOL. 23, PA4206, doi:10.1029/2008PA001637, 2008

Sahel megadroughts triggered by glacial slowdowns of Atlantic meridional overturning

Stefan Mulitza,[1] Matthias Prange,[1] Jan-Berend Stuut,[1] Matthias Zabel,[1] Tilo von Dobeneck,[1] Achakie C. Itambi,[1] Jean Nizou,[1] Michael Schulz,[1] and Gerold Wefer[1]

Received 22 April 2008; revised 24 July 2008; accepted 2 September 2008; published 28 October 2008.

[1] The influence of the large-scale ocean circulation on Sahel rainfall is elusive because of the shortness of the observational record. We reconstructed the history of eolian and fluvial sedimentation on the continental slope off Senegal during the past 57,000 years. Our data show that abrupt onsets of arid conditions in the West African Sahel were linked to cold North Atlantic sea surface temperatures during times of reduced meridional overturning circulation associated with Heinrich Stadials. Climate modeling suggests that this drying is induced by a southward shift of the West African monsoon trough in conjunction with an intensification and southward expansion of the midtropospheric African Easterly Jet.

Citation: Mulitza, S., M. Prange, J.-B. Stuut, M. Zabel, T. von Dobeneck, A. C. Itambi, J. Nizou, M. Schulz, and G. Wefer (2008), Sahel megadroughts triggered by glacial slowdowns of Atlantic meridional overturning, *Paleoceanography*, *23*, PA4206, doi:10.1029/2008PA001637.

1. Introduction

[2] Life in the semiarid Sahel belt of tropical North Africa strongly depends on the availability of water and has been frequently affected by shifts to more arid climate, at least since the Pliocene [*deMenocal*, 1995]. The most recent drought occurred in the early 70s and 80s of the last century with partial recovery during the late 90s [e.g., *Nicholson*, 2000]. Historical records suggest that Sahel droughts result from changes in the large-scale distribution of sea surface temperature [e.g., *Lamb*, 1978; *Folland et al.*, 1986] which (among other factors) is influenced by the heat transport due to the Atlantic meridional overturning circulation (AMOC) [*Newell and Hsiung*, 1987]. The contribution of the AMOC to the long-term variability of Sahel precipitation has not yet been demonstrated. Since the AMOC underwent substantial variations during the late Quaternary [*McManus et al.*, 2004], high-resolution sediment records from ocean margin settings offer the opportunity to study the response of continental climate to changes in ocean circulation.

[3] The continental slope off Northern Senegal is an ideal site to study the history of Sahel drought, because it records the varying input of eolian dust and fluvial sediments from the adjacent African continent [*Koopmann*, 1981; *Sarnthein et al.*, 1981] (Figure 1). Dust with particle sizes up to 200 μm [*Stuut et al.*, 2005] is mobilized in the Sahel and the western Sahara [*Grousset et al.*, 1998; *Jullien et al.*, 2007] and transported offshore mainly by continental trade winds and the Saharan Air Layer [*Prospero and Carlson*, 1981]. Recent ship-based dust samples collected off Senegal and Mauritania between 13 and 20°N indicate that 44–83% of the dust is deposited at grain sizes larger than 10 μm [*Stuut et al.*, 2005]. By contrast, 95% of the terrigenous sediments delivered by the Senegal River have grain sizes below 10 μm [*Gac and Kane*, 1986]. The Fe/K ratio of atmospheric dust samples [*Stuut et al.*, 2005] shows a close relation to precipitation, with values around 2.01 (~28°N–14°N, n = 7, SD = 0.41) in the Sahel-Saharan area and values around 3.88 (~6°N–7°S, n = 11, SD = 0.41) in the tropics (Figure 2). This increase in Fe/K ratios toward the tropics reflects the increasing amount of dust derived from deeply chemically weathered terrains [*Moreno et al.*, 2006] with relatively high concentrations of iron and aluminum in comparison to the more mobile potassium.

[4] The material transported with the Senegal River also has a very distinct geochemical signature (Table 1). Compared to the chemical composition of atmospheric dust in the Sahel [*Orange et al.*, 1993; *Stuut et al.*, 2005], suspended sediments in the Senegal River show significantly higher Fe/K and Al/Si ratios [*Gac and Kane*, 1986].

[5] The Senegal River mainly drains the western part of Guinea. Sediment input from the Senegal River is highly dependent on the total water discharge and mainly occurs during the rainy summer season [*Kattan et al.*, 1987]. Both dust mobilization and fluvial input are controlled by the background climate; the most recent multidecadal Sahel drought has been associated with an increase in dust mobilization and export over the Atlantic [*Prospero and Lamb*, 2003] and a decrease in Senegal River discharge by more than 50% with respect to the long-term mean [*Kattan et al.*, 1987].

[6] Here we present a 57-ka-long record of terrigenous sedimentation from the continental slope off Senegal, westward of the Senegal River mouth. Variations in the composition of the terrigenous material indicate that Sahel

[1]Marum and Department of Geosciences, University of Bremen, Bremen, Germany.

0883-8305/08/2008PA001637$12.00

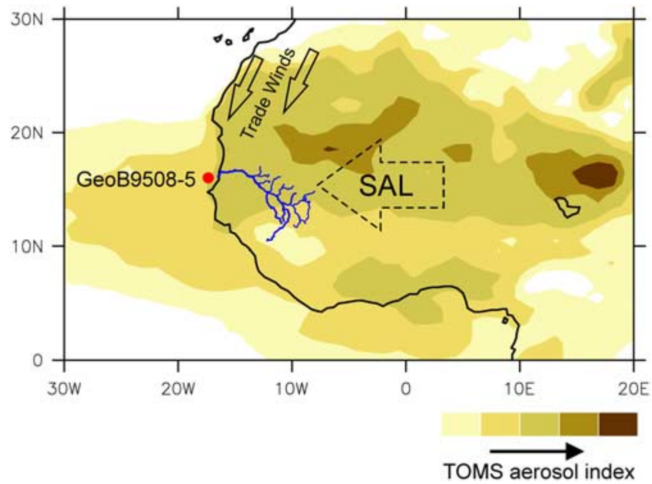

Figure 1. Position of gravity core GeoB9508–5 (red dot) close to the mouth of the Senegal River (blue) and Total Ozone Mapping Spectrometer (on Nimbus 7) (TOMS) averaged aerosol concentrations for the years 1997–2005 highlighting the Sahara-Sahel Dust Corridor (TOMS data are available at http://toms.gsfc.nasa.gov/). Arrows indicate principal wind directions of trade winds and Saharan Air Layer (SAL).

megadroughts occurred during Heinrich Stadials and were associated with cold North Atlantic sea surface temperatures during times of reduced meridional overturning circulation. We study the physics behind the changes in West African hydrology by means of a freshwater-hosing experiment using a fully coupled climate model. Our model results suggest that North Atlantic sea surface temperature and West African rainfall are linked through shifts in the positions of the monsoon trough and the midtropospheric African Easterly Jet.

2. Material and Methods

2.1. Measurements on Core GeoB9508–5

[7] Our 965-cm-long gravity core GeoB9508–5 was retrieved from the continental slope off Senegal at about 15°29.90N/17°56.88W from 2384 m water depth (Figure 1). Bulk sediment samples were taken every 2.5 cm downcore, washed over 150 and 63 μm sieves and dried in an oven at 60°C. From the size fraction >250 μm of each sample, 1–10 specimens of *Cibicidoides wuellerstorfi* were picked for isotope analyses. The isotopic composition of the foraminiferal shells was measured using a Finnigan MAT 252 mass spectrometer equipped with an automatic carbonate preparation device. The working standard gas (Burgbrohl CO_2) was calibrated against Vienna PDB (VPDB) by using the National Bureau of Standards (NBS) 18, 19 and 20 standards. Internal precision, based on replicates of an internal limestone standard, was better than 0.07‰. From the total of 391 measurements, 10 outliers were rejected.

[8] The age model of core GeoB9508–5 is based on 12 radiocarbon ages on mixed samples of planktonic foraminifera picked from the >150 μm fraction. All dates were measured at the Leibniz-Laboratory for Radiometric Dating and Stable Isotope Research in Kiel. Raw ages were corrected for a reservoir age of 400 years; they were then converted to calendar ages using the "Fairbanks0107" calibration curve [*Fairbanks et al.*, 2005] for ages smaller than 40,000 (Table 2). Seven additional age points were introduced between the fixed radiocarbon ages by alignment to the benthic δ^{18}O record of core MD95–2042 [*Shackleton et al.*, 2004] (Figure 3a).

[9] Samples for grain size analyses were taken every 5 cm downcore. In order to isolate the terrigenous fraction from the deep marine sediments, several pretreatment steps were undertaken to remove different biogenic constituents. Organic carbon was removed by adding 10 ml H_2O_2 (35%) to approximately 750 mg of bulk sediment. Reaction was sped up by boiling the mixture. Boiling was continued until reaction stopped and excess H_2O_2 was decomposed into H_2O and O_2. Subsequently, $CaCO_3$ was removed by boiling the sediment sample in 100 ml demineralized water for 1 min with 10 ml HCl (10%). The sample was diluted with demineralized water until pH = 7. Subsequently, biogenic opal was removed by adding 6 g NaOH to the sample in 100 ml water, and boiled for 10 min. The sample was diluted again with demineralized water until pH = 7. As a last step before the analysis, the sediment sample in 100 ml was boiled shortly with 300 mg of the dispersing agent $Na_4P_2O_7*10H_2O$. All samples were measured with a Coulter laser particle sizer LS200, resulting in 92 size classes from 0.4–2000 μm at a 5 cm ($\sim$250 years) downcore sampling interval.

[10] Samples for geochemical measurements were taken at 4 cm intervals. The sediment material was dried at 200°C, powdered and homogenized. Single element concentrations were determined on 4 g of dry subsamples by energy dispersive polarization X-ray fluorescence (EDP-XRF)

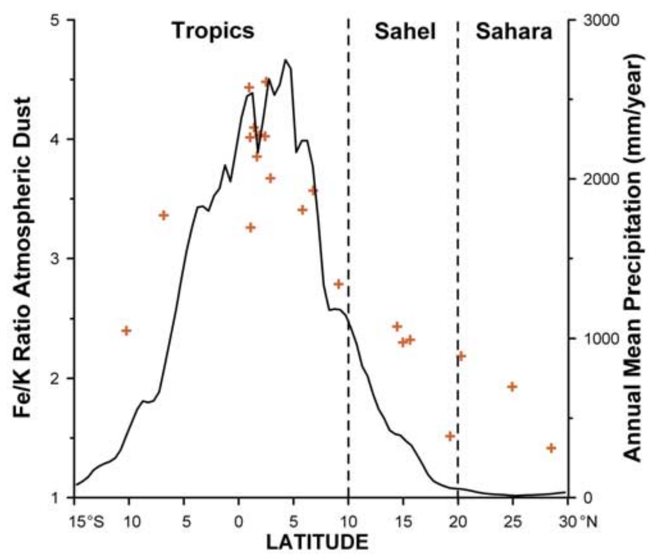

Figure 2. Comparison of Fe/K of atmospheric dust sampled in the period from February–March 1998 on R/V *Meteor* along western Africa (data from *Stuut et al.* [2005]) and annual mean precipitation at 18°W (*Global air temperature and precipitation* are available at http://climate.geog.udel.edu/~climate/html_pages/archive.html).

Table 1. Mean Fe/K and Al/Si Ratios of Suspended Matter From the Senegal River Mouth[a]

	Senegal River Suspension[b]	Dust (Dakar)[c]	Dust (Offshore Senegal)[d]
Fe/K	4.83 (n = 10, SD = 0.28)	2.93 (n = 4, SD = 1.33)	2.35 (n = 3, SD = 0.07)
Al/Si	0.55 (n = 10, SD = 0.03)	0.18 (n = 4, SD = 0.03)	-

[a]Samples were taken in the period from August 1981 to November 1982 [*Gac and Kane*, 1986] of atmospheric dust in Dakar (mean of yearly averages from 1984 to 1987 from *Orange et al.* [1993]) and atmospheric dust offshore Senegal [*Stuut et al.*, 2005] close to the position of GeoB9508–5. n, number of observations; SD, standard deviation.
[b]Data taken from *Gac and Kane* [1986].
[c]Data taken from *Orange et al.* [1993].
[d]Data taken from *Stuut et al.* [2005].

spectroscopy using a SPECTRO XEPOS instrument (see *Wien et al.* [2005] for a detailed description of the setup). The device was operated with the software Spectro X-Lab Pro (Version 2.4), using the Turboquant method [*Schramm and Heckel*, 1998]. Analytical quality was assessed by repeated analyses of the certified standard reference material MAG-1 [*Govindaraju*, 1994]. The measured values were within 2% of the accepted value for Si, Al, K, Ca, and Fe and within 5% for Ti. The standard deviation of replicates was less than 2%.

2.2. Setup of Model Experiments

[11] Numerical experiments were performed with an adjusted version of the "paleo release" of the NCAR (National Center for Atmospheric Research) Community Climate System Model CCSM2.0.1. The global climate model is composed of four components representing atmosphere, ocean, land, and sea ice. The resolution of the atmospheric component is given by T31 (3.75° by 3.75° transform grid) spectral truncation for 26 layers, while the ocean has a mean resolution of 3.6° by 1.6° with 25 levels. The latitudinal resolution of the oceanic model grid is variable, with finer resolution near the equator (~0.9°). This version of CCSM2.0.1 is referred to as CCSM2/T31x3a [*Prange*, 2008].

[12] A control run was performed in which we adopted the atmospheric composition of 1990 AD and initialized the model with modern observational data sets. An asynchronous integration technique was used to achieve a statistical equilibrium of the climate system within 300 years of model integration [*Prange*, 2008]. This spin-up phase was followed by a 200-year-long synchronous integration, the second half of which serves for model-data analysis of the control climate in the present study.

[13] The present-day control run was perturbed by a freshwater flux of 0.1 sverdrup (Sv, 10^6 m^3 s^{-1}) into high northern seas. The surface freshwater forcing was applied to the Labrador Sea, the Nordic Seas, the Arctic Ocean as well as the Hudson and Baffin bays. The continuously perturbed model was integrated (synchronously) for almost 450 years. Averages over the last 100 years of the water-hosing experiment were used for further analysis.

3. Results

3.1. Downcore Variability of Benthic $\delta^{18}O$, Grain Size, and Elemental Ratios

[14] The age model of the core indicates an age at the base of the core of about 57 ka and mean sedimentation rates of about 17 cm ka^{-1}. Between about 57 and 15 ka B.P., the benthic $\delta^{18}O$ record is characterized by a series of events with relatively low benthic $\delta^{18}O$ values (Figure 3). It has been previously shown [*Shackleton et al.*, 2000] that these events coincide with warm temperatures over Antarctica, the so-called Antarctic Isotope Maxima (AIM) [*European Programme for Ice Coring in Antarctica* (*EPICA*), 2006] (Figures 4d and 4e), and are probably due to a combination of ice volume and deep-water temperature changes that occur synchronously with temperature changes over Antarctica.

[15] The Holocene section of this core contains only small amounts of coarse-grained dust (Figure 3b). Al/Si and Fe/K ratios are highest in the mid-Holocene, when the values are very close to the modern composition of Senegal River suspension (Figure 4 and Table 1). Both ratios decrease gradually toward the present.

[16] The glacial section of the downcore record of GeoB9508–5 is characterized by a series of abrupt increases in grain size associated with decreases of Al/Si and Fe/K ratios starting at about 49, 41, 31, 26, 19 and 13 ka B.P (Figures 3 and 4). These events coincide with the most prominent Antarctic Isotope Maxima (AIMs 1, 2, 8, 12) and

Table 2. Radiocarbon Dates and Age Model of Core GeoB9508–5[a]

Sample Code	Core Depth (cm)	^{14}C AMS age (−400) (ka B.P.)	Error (years)	Calendar Age (ka B.P.)
KIA 31283	3	520	30/30	531
KIA 31282	68	5745	50/50	6533
KIA 33724	98	8830	60/60	9900
KIA 33725	123	10,160	80/80	11,830
KIA 33726	163	11,080	80/80	12,940
	172[b]			14,600
	236[b]			15,800
KIA 31770	308	16,250	90/90	19,373
KIA 31769	343	19,190	120/120	22,789
KIA 31768	388	21,630	120/120	26,021
KIA 31766	483	26,410	210/200	31,674
	513[b]			33,370
KIA 31765	583	31,690	350/340	37,069
	603[b]			38,680
KIA 31764	663	36,600	640/590	41,785
	753[b]			47470
KIA 31281	778	42,940	1660/1370	-
	923[b]			56,070
	953[b]			57,120

[a]AMS ages were corrected by a reservoir age of 400 years and then converted to calendar ages using the Fairbanks0107 calibration curve [*Fairbanks et al.*, 2005]. AMS, Accelerator Mass Spectrometer.
[b]Ages were derived by correlation to the benthic $\delta^{18}O$ record of core MD95–2042 [*Shackleton et al.*, 2004].

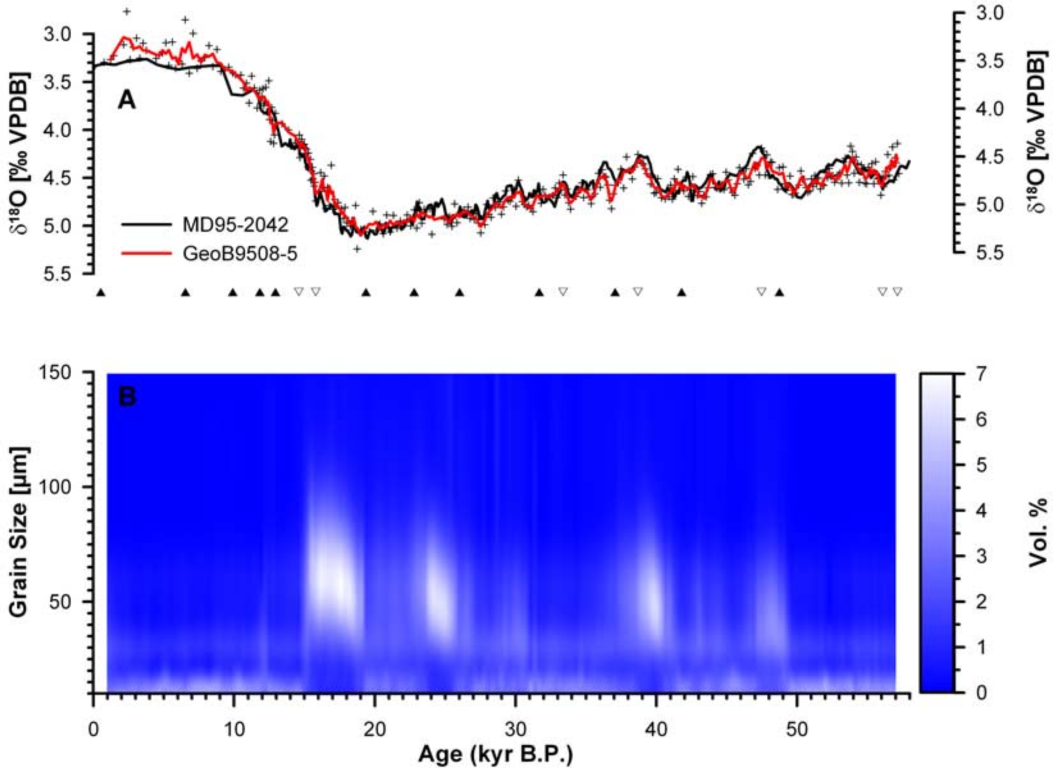

Figure 3. (a) Benthic $\delta^{18}O$ record of cores GeoB9508–5 (this paper) and MD95–2042 [*Shackleton et al.*, 2004]. (b) Grain size distribution in core GeoB9508–5 (this paper). Filled triangles indicate Accelerator Mass Spectrometer radiocarbon datings, and open triangles indicate age points derived by correlation with the benthic $\delta^{18}O$ record of core MD95–2042. The red curve is a three-point running mean of the benthic $\delta^{18}O$ data (crosses).

their Northern Hemisphere counterparts, the Heinrich Stadials 1–5 and the Younger Dryas.

[17] During the Heinrich Stadials both low Al/Si and Fe/K ratios and the low amount of fine material (<20%) are consistent with the deposition of atmospheric dust and indicate a reduced contribution from Senegal River suspension. Generally, the amount of fine material (<10 μm) is highly correlated (R^2 = 0.9 when interpolated to 500-year intervals) with Al/Si ratios.

3.2. Modern Atmospheric Circulation in CCSM2/T31×3a

[18] CCSM2/T31×3a simulates a robust Atlantic overturning circulation. Approximately 10 Sv of deepwater formed in the North Atlantic are exported to the Southern Ocean. A detailed description of the overall model performance in simulating the global climatology and ocean circulation can be found elsewhere [*Prange*, 2008].

[19] For the present study, the model's skill in simulating the West African monsoon circulation is of paramount importance. Recently, a comprehensive analysis of coupled general circulation models (CGCMs) revealed that many global state-of-the-art models failed to capture the major features of the West African monsoon circulation under modern boundary conditions [*Cook and Vizy*, 2006]. Eight of the 18 examined CGCMs did not even reproduce the summer migration of the tropical rain belt onto the West African continent. Figure 5a shows climatological near-surface winds and precipitation over West Africa for the summer season July–September as derived from reanalysis [*Kalnay et al.*, 1996] and observational [*Legates and Willmott*, 1990] data, respectively. Transporting moisture onto the continent across the Guinean coast, the northward low-level monsoon flow penetrates as far north as 20°N, where it converges with dry northerly winds at the monsoon trough. Summer precipitation over West Africa has two distinct regional maxima. One is centered on the west coast between ~5°N and ~12°N, another is near the Cameroon highlands in the eastern Guinea coastal region. Both the wind and precipitation patterns are rather well captured by CCSM2/T31×3a (Figure 5b). Even though the winds over the Sahara are somewhat stronger than in the reanalysis, their flow direction is satisfactorily simulated. Convergence with the southerly monsoon winds takes place at ~20°N. Summer precipitation maxima reside on the African continent. The location of the west coast maximum is fairly well reproduced, albeit the amount of rainfall is underestimated by the model. The Cameroon maximum is also too weak and too far inland.

[20] In winter (January–March) the northerly dry Harmattan winds penetrate as far south as ~10°N in the reanalysis data (Figure 5c). In the Sahel, observed rainfall

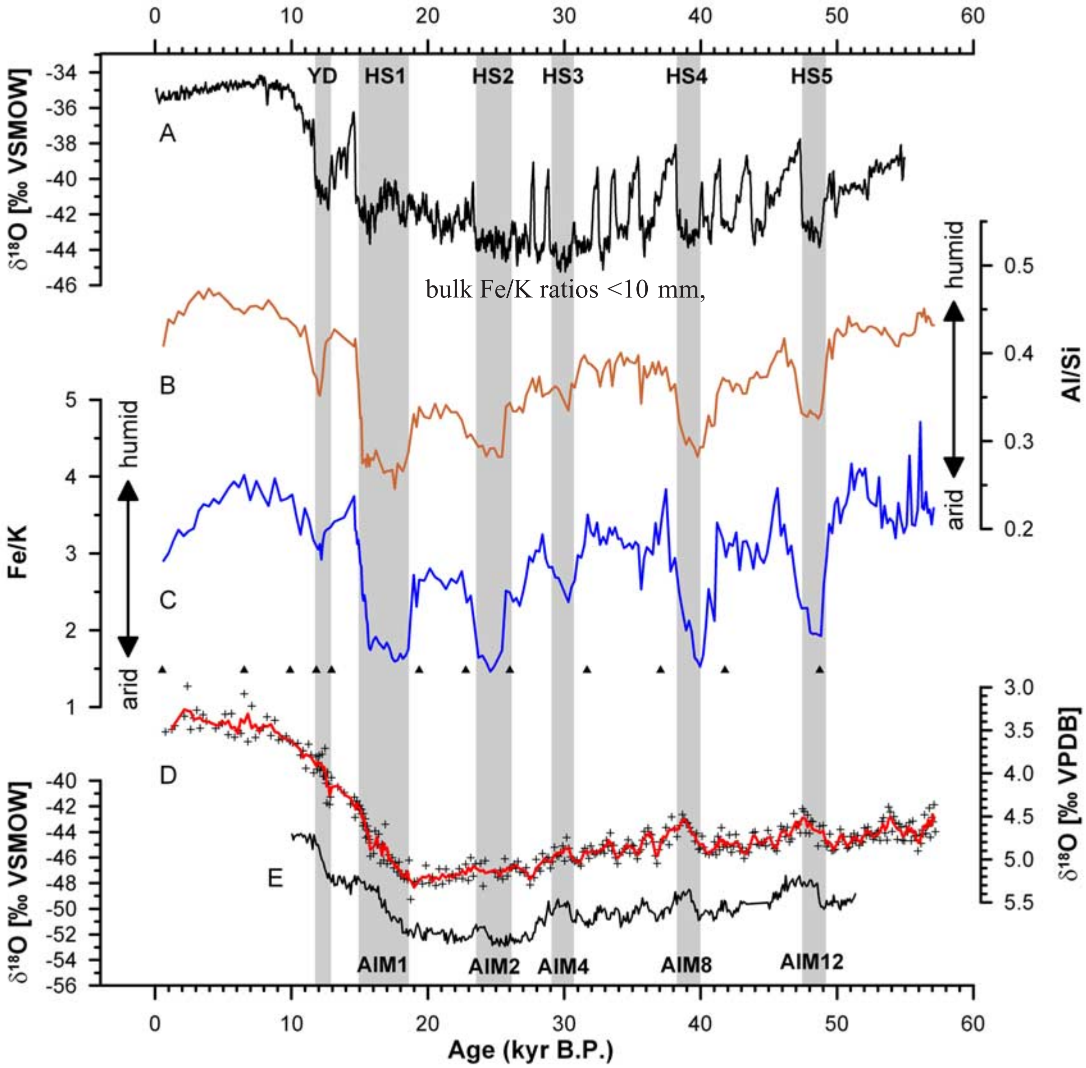

Figure 4. Comparison of sedimentary records of core GeoB9508–5 with (a) d^{18}O of Greenland (North Greenland Ice core Project) and (e) Antarctic (EPICA Dronning Maud Land) ice cores versus time [EPICA, 2006]. (b) Bulk Al/Si ratios, (c) bulk Fe/K ratios, and (d) oxygen isotope record of benthic foraminifera in core GeoB9508–5 Gray bars indicate the approximate occurrence of Dansgaard-Oeschger Stadials associated with Heinrich Events (i.e., Heinrich Stadials (HS)) and the Younger Dryas (YD) in the Northern Hemisphere and the corresponding Antarctic Isotope Maxima in the Southern Hemisphere.

approaches zero, while the zonal band of maximum rainfall is located over the Gulf of Guinea. Even though the Harmattan winds are stronger and penetrate farther south in the CCSM2/T31×3a control run, the overall patterns of low-level winds and rainfall are well simulated (Figure 5d).

[21] The atmospheric circulation at higher tropospheric levels is also well captured by CCSM2/T31×3a. Figure 6 shows a cross section of the mean zonal wind velocity on the Greenwich meridian from reanalysis data and model output for the summer season. The West African monsoon is depicted as a low-level westerly flow. Above the low-level westerlies is the African Easterly Jet (AEJ) with maximum wind speeds between 700 and 500 hPa. The African Easterly Jet is the equatorward portion of the Saharan High, the divergence center that overlays the near-surface continental thermal low in both the model and the reanalysis data. In the upper troposphere (higher than 300 hPa) the lowermost part of the Tropical Easterly Jet (TEJ) is visible in both the model and reanalysis data.

[22] Compared to climatological data, summer rainfall is undersimulated south of ~15°N and somewhat too high to the north of it. In CCSM2/T31×3a, 65% of the annual rainfall in the West African Sahel (i.e., west of 10°E in the latitude belt 10°N–20°N) occurs during the summer months July–September, while only 1.5% takes place during January–March. The precipitation climatology [*Legates and Willmott*, 1990] suggests that about 70% (1%) of the annual West African Sahel rainfall occurs

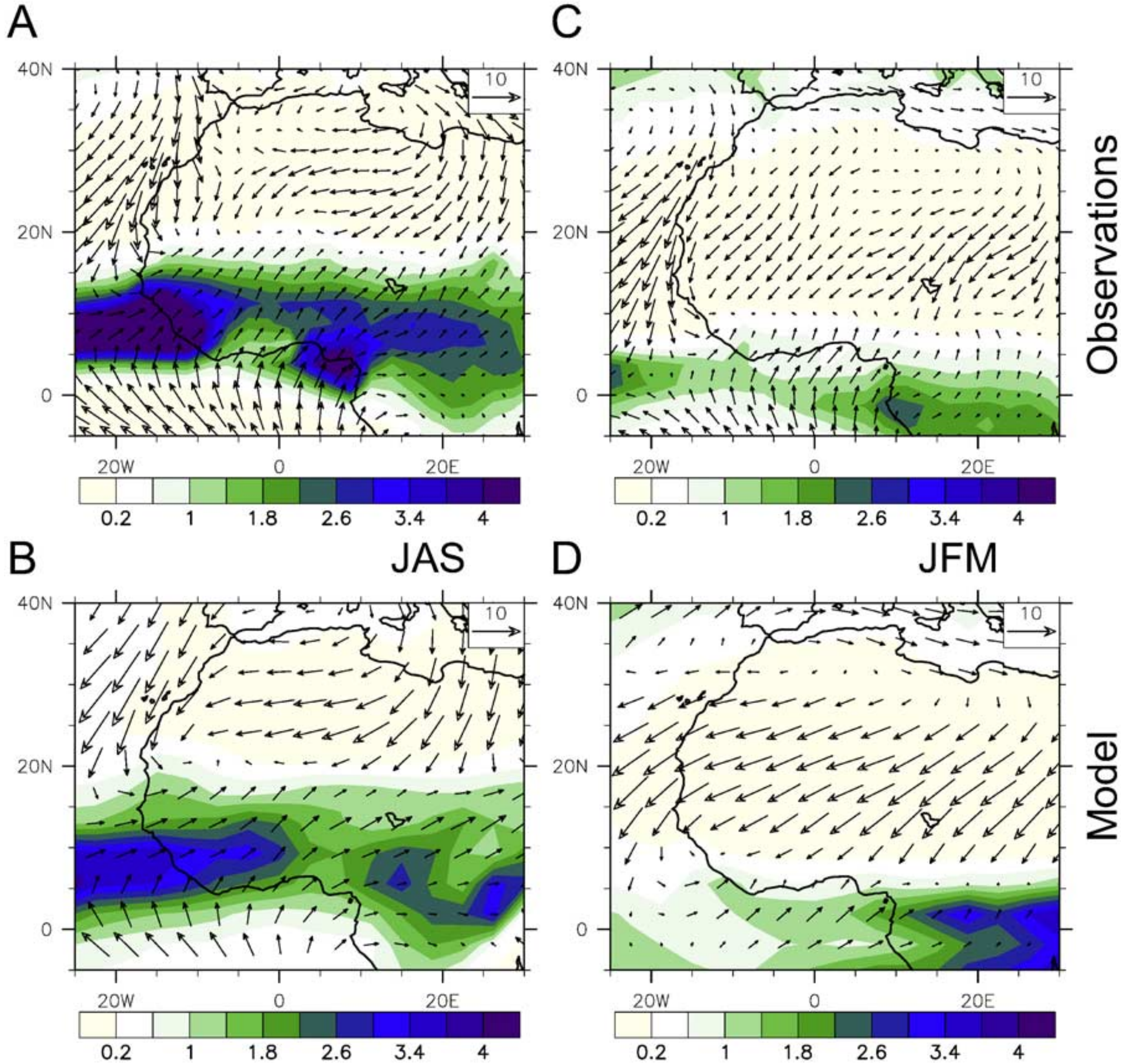

Figure 5. Mean precipitation (m a^{-1}) and near-surface winds (m s^{-1}) over West Africa for (a, b) July–September and (c, d) January–March as calculated from observational/reanalysis data (Figures 5a and 5c) and the CCSM2/T31x3a control run (Figures 5b and 5d). The land data for the precipitation climatology are based on historical rain gauge measurements [*Legates and Willmott*, 1990]. Winds are taken from the National Centers for Environmental Prediction (NCEP)/National Center for Atmospheric Research (NCAR) reanalysis data set [*Kalnay et al.*, 1996] and averaged over the entire reanalysis period (1948–2006). The model results represent averages over the last 100 years of the control run.

during July–September (January–March). In summary, CCSM2/T31×3a simulates a realistic West African monsoon circulation and captures the major features of the West African precipitation climatology.

3.3. Response of the Atmospheric Circulation to AMOC Slowdown

[23] The continuous but small (0.1 Sv = $0.1 \cdot 10^6$ m^3 s^{-1}) freshwater input to the northern North Atlantic and Arctic Oceans induces a gradual decline of the AMOC. Deepwater formation in the North Atlantic slowly decreases and eventually falls below 2 Sv after ~300 years of integration. The maximum northward heat transport in the North Atlantic decreases from 0.6 PW [*Prange*, 2008] to 0.32 PW in the hosing experiment. In the South Atlantic, the heat transport even changes its direction (i.e., it becomes southward in response to the freshwater perturbation). Summer precipitation and runoff over the West African Sahel parallels the decrease of the AMOC and the associated heat transport, suggesting an almost linear relationship between overturning strength and Sahel rainfall (Figure 7). The simulated drying is not restricted to the Sahel. Rather, it affects the entire West African region including the Guinea coast (Figure 8a). The slowing of the AMOC induces surface cooling in the North Atlantic realm which extends far over Europe, the Mediterranean, and northern North Africa (Figure 9). During summer (July–September), the associated positive sea level pressure anomaly results in a southward

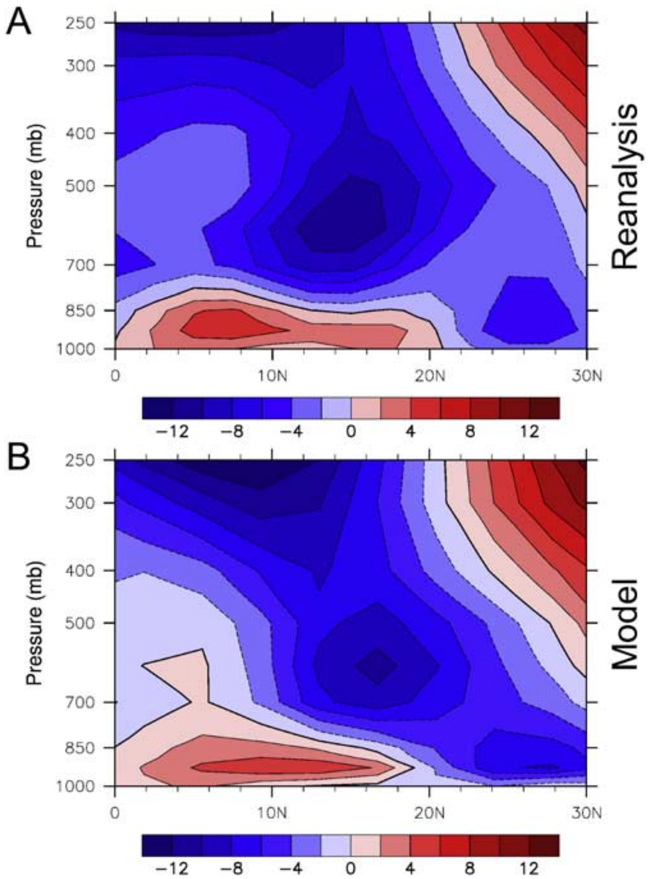

Figure 6. Latitude-height cross sections of July–September mean zonal wind velocity (m s^{-1}) over West Africa along the Greenwich meridian from the (a) NCEP/NCAR reanalysis and the (b) CCSM2/T31×3a control run. NCEP/NCAR winds are averaged over the entire reanalysis period (1948–2006), while the model result represents an average over the last 100 years of the control run. Positive (negative) values indicate westerly (easterly) flow.

shift of the West African monsoon trough (also referred to as the Intertropical Convergence Zone) by about 3–4° latitude (Figure 8b). As a result, monsoonal rainfall retreats from the northern portion of the West African Sahel. Reduced evapotranspiration from the drier land surface (a reduction of ~10 W m^{-2} in averaged summer surface latent heat flux over the West African Sahel) and less cloudiness (plus ~15 W m^{-2} of averaged summer net solar flux at the surface) amplify the Sahel surface warming which is initiated by the anomalous southward low-level transport of warm Saharan air (note that reduced latent heat and enhanced shortwave fluxes at the surface are essentially balanced by increased sensible heat and net longwave fluxes). This warming results in a steepening of the meridional surface temperature gradient between the Sahel and the relatively cool Guinean coast. According to the thermal wind balance, the zonal midlevel circulation intensifies at the altitude of the African Easterly Jet (Figures 8c and 10). Near 15°N, where the surface wind anomaly converges (Figure 8b), an anomalous ascent of air occurs below the level of condensation. This upward flow supplies the anomalous easterly midlevel jet with relatively dry air from the north, while over southern West Africa, the accelerated midlevel easterly flow enhances the export of moisture from the continent to the Atlantic Ocean (Figure 8d). The enhanced moisture divergence is associated with a further reduction in rainfall over West Africa.

[24] The annual rainfall over the West African Sahel decreases by ~25% in our water hosing experiment. This value is comparable to the precipitation decrease that took place during the recent Sahel drought of the 1970s/80s. Basically, drying of the Sahel takes place in all seasons in the hosing experiment. However, since the major portion of Sahel rainfall occurs during July–September (see above), the summer response of the African hydrological cycle to AMOC slowdown is by far most important.

4. Discussion

[25] Today terrigenous sediments deposited on the continental slope of Senegal mainly stem from atmospheric dust and river input. These transport processes signify two different precipitation regimes: dust input mainly occurs during dry conditions whereas river input occurs when precipitation is high in the drainage basin of the Senegal River. Since our core is located at the boundary between both regimes it reflects the relative proportions of fluviatile and eolian sediments and should be a sensitive recorder of

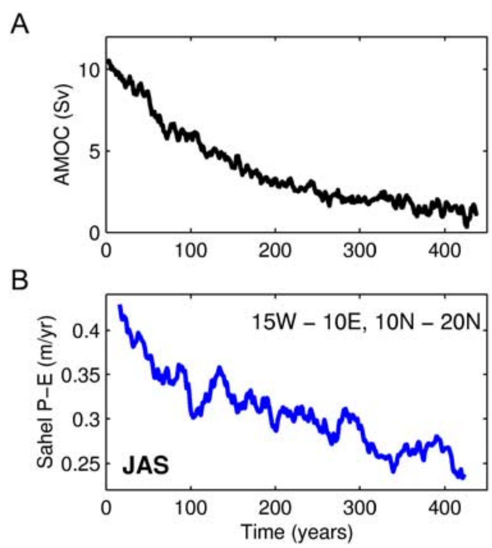

Figure 7. Results from the coupled general circulation models (CGCM) water-hosing simulation where the high northern seas are perturbed by a continuous freshwater input of 0.1 Sv. (a) Temporal evolution of the Atlantic meridional overturning circulation (AMOC), starting from the equilibrium climate of the control run. Shown is the maximum of the overturning stream function north of 40°N smoothed with a 5-year boxcar average. (b) Summer, i.e., July/August/September (JAS), net precipitation (total precipitation minus evapotranspiration) averaged over the West African Sahel (15°W–10°E, 10°N–20°N) smoothed with a 30-year boxcar average.

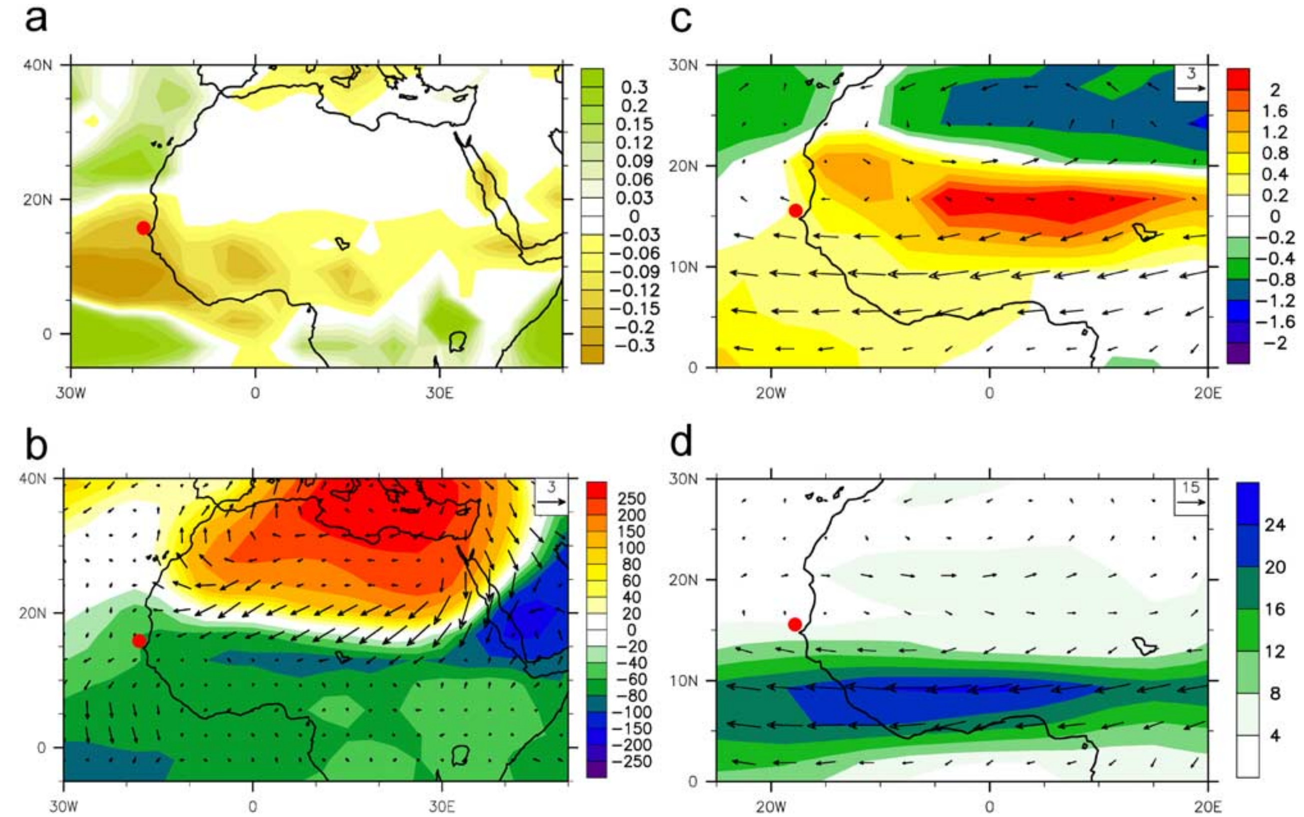

Figure 8. African climate response to a substantial weakening of the AMOC in a CGCM water-hosing experiment. Shown are differences between the climate state with weak AMOC (averages over the last 100 years of the water-hosing experiment) and the state with strong AMOC (100-year averages from the control run). The red dot indicates the position of core GeoB9508–5. (a) Annual net precipitation (total precipitation minus evapotranspiration in m a^{-1}), (b) summer (JAS) sea level pressure (Pa) and near-surface winds (m s^{-1}), (c) summer (JAS) surface temperature (°C) and winds at 700 hPa (m s^{-1}), and (d) summer (JAS) moisture transport at 700 hPa (contours indicate the magnitude of the moisture transport in g kg^{-1} m s^{-1}).

Sahel precipitation. This interpretation is consistent with the general decrease of Al/Si and Fe/K ratios during the late Holocene along with a gradual drying trend over North Africa in response to weakening insolation forcing [e.g., *Kröpelin et al.*, 2008].

[26] The salient feature in gravity core GeoB9508–5 is series of abrupt increases in grain size associated with decreased Al/Si and Fe/K ratios. These events must be interpreted as periods with much lower sediment discharge from the Senegal River together with an increase in atmospheric dust input as a consequence of drought. Geomorphological evidence for a much drier climate in much of northern Senegal is given for the most recent multimillennial period of drought, occurring between about 19 and 15 ka B.P at the onset of the last deglaciation. During this time much of Senegal was covered by the so-called Ogolian Dunes [*Michel*, 1973]. The presence of these dunes as far south as 14°N suggests a southward shift of the corresponding climate zone by 4–5° and provides additional evidence for aridity in the West African Sahel. Further evidence for aridity in the Sahel, at least during the Younger Dryas, comes from several lake records [*Gasse and van Campo*, 1994; *Gasse*, 2000].

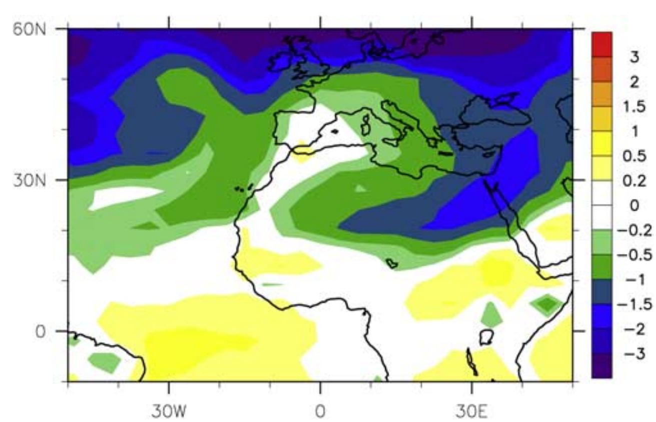

Figure 9. Response of the annual mean surface temperature (°C) to a substantial weakening of the AMOC in the water-hosing experiment. Shown is the difference between the climate state with weak AMOC (average over the last 100 years of the hosing experiment) and the state with strong AMOC (100-year average from the CCSM2/T31×3a control run).

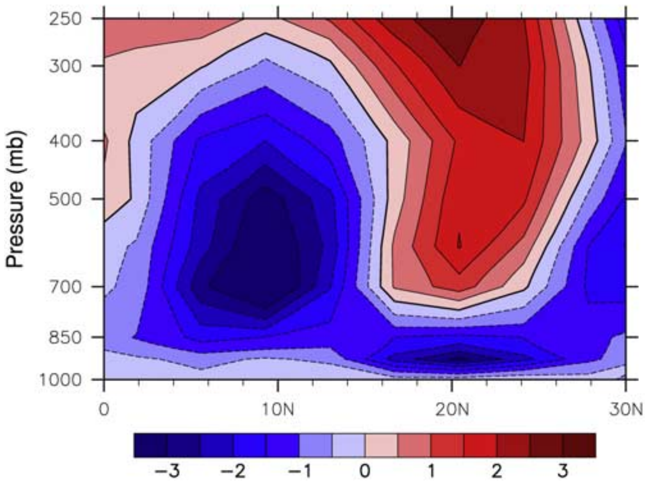

Figure 10. Response of the July–September mean zonal wind velocity (m s^{-1}) to a substantial weakening of the AMOC, plotted as a latitude-height cross section along the Greenwich meridian. Shown is the difference between the climate state with weak AMOC (average over the last 100 years of the water-hosing experiment) and the state with strong AMOC (100-year average from the CCSM2/T31$\times$3a control run). Positive (negative) values indicate westerly (easterly) wind anomalies.

[27] Within the accuracy of the age model the repeated and abrupt initiation of dry Sahel climates occurs synchronously with the coldest sea surface temperatures in the northeastern Atlantic during the past 60 ka [*de Abreu et al.*, 2003]. These extremely cold sea surface temperatures only occur during Dansgaard-Oeschger Stadials associated with ice rafting (Heinrich) Events in the Northern Hemisphere. The longest drought with an approximate duration of about 4 ka occurs at the onset of the last deglaciation together with Heinrich Stadial 1 in the North Atlantic [*Sarnthein et al.*, 2000] and a pronounced warming (AIM 1) of the same duration over Antarctica [*EPICA*, 2006] (Figure 4e). It is generally accepted [*EPICA*, 2006] that the antiphasing of temperatures over Greenland and Antarctica is due to reductions in the AMOC with a decrease of the heat export from the South Atlantic to the North Atlantic and a subsequent cooling of much of the North Atlantic surface. Hence, our data strongly suggest a relation between the strength of the AMOC and sea surface temperature in the North Atlantic on the one hand and Sahel precipitation on the other hand.

[28] Previous studies [e.g., *Street-Perrott and Perrott*, 1990; *Mulitza and Rühlemann*, 2000; *Chiang and Koutavas*, 2004; *Dahl et al.*, 2005; A. C. Itambi et al., Millennial-scale northwest African droughts relates to H events and D O Cycles: Evidence in marine sediments from off-shore Senegal, submitted to *Paleoceanography*, 2008] interpreted drought in the tropics by a southward shift of the Intertropical Convergence Zone (ITCZ). Our experiments indeed suggest a southward shift of the ITCZ (i.e., monsoon trough) during AMOC slowdown by a few degrees latitude over West Africa. It is however problematic to explain the widespread nature of drought exclusively with an ITCZ shift. Today, the ITCZ seems to be effectively independent of the system that produces most of the rainfall. The tropical rainbelt (which is often confused with the ITCZ) is in fact produced by a deep core of ascent lying between the axes of the AEJ and the TEJ, some ten degrees of latitude south of the ITCZ [*Nicholson and Grist*, 2003]. Interestingly, a southward shift of the ITCZ has been rejected as a cause of the multidecadal Sahel drought during the second part of the last century [*Citeau et al.*, 1989].

[29] Also, a southward shift of the ITCZ as the sole reason for drought would require increased precipitation to the south of the present-day ITCZ. Such a pattern would be in disagreement with late Quaternary paleolimnological records from Lake Bosumtwi ($\sim$6°N), Ghana, which indicate dry conditions at the Guinean coast during millennial-scale periods of reduced AMOC [*Peck et al.*, 2004; *Shanahan et al.*, 2006]. Likewise, paleoceanographic records off Nigeria ($\sim$3°N) [*Weldeab et al.*, 2007], Congo ($\sim$6°S) [*Schefuß et al.*, 2005] and Angola ($\sim$12°S) [*Dupont et al.*, 2008] do not show indications of increased precipitation during Heinrich Stadials. The simulated drying in our water hosing experiment is not restricted to the Sahel. Rather, it affects the entire West African region including the Guinea coast (Figure 5a) in agreement with the paleoclimatic evidence, but in contrast to the simulation of *Dahl et al.* [2005]. For this reason, the proposed mechanism which involves an intensified moisture export by the midlevel African Easterly Jet is a reasonable explanation for the observed precipitation pattern.

[30] It must be noted that our model setup includes a comprehensive land surface component with sophisticated soil-vegetation biogeophysics and hydrology [*Bonan et al.*, 2002; *Oleson et al.*, 2004], but fixed vegetation. An interactive vegetation cover would likely worsen the simulation of the present monsoon climatology. Prescribing the vegetation provides for a more reliable simulation of the climatology, although potentially important feedbacks are excluded in the water-hosing experiment. Even though vegetation-climate feedbacks could conceivably act to amplify the response of Sahel precipitation to a remotely forced perturbation [*Charney*, 1975; *Zeng et al.*, 1999], there is no obvious reason why the basic dynamical mechanisms of Sahel drying deduced from our CGCM water-hosing experiment should be affected fundamentally by vegetation dynamics [cf. *Hales et al.*, 2006]. We also note that the assumption of a strong positive vegetation-precipitation feedback over northern Africa has recently been challenged [*Levis et al.*, 2004; *Liu et al.*, 2007, 2006; *Wang et al.*, 2008]. Essentially, the same holds for dust radiative feedbacks [*Yoshioka et al.*, 2007]. Excluding vegetation and dust feedbacks, our approach can be considered as a "maximum simplicity model" to simulate a physically consistent mechanism of Sahel drying in response to a weakening of the AMOC.

[31] In the present study, no attempts have been made to simulate and perturb a glacial climate state. Simulations of glacial West African climate can hardly be validated. Moreover, it has recently been shown that the simulation of glacial African rainfall is mostly model dependent [*Braconnot et al.*, 2007]. Within the framework of the

Paleoclimate Modeling Intercomparison Project PMIP-2, simulations of the Last Glacial Maximum with five different CGCMs yielded summer Sahelian rainfall anomalies ranging between −42% and +16% depending on the model. We therefore suspect that trustworthy simulations of the glacial West African monsoon dynamics are currently not available. As a note of caution, however, we emphasize again that varying boundary conditions (i.e., ice sheet distribution, orbital parameters, atmospheric composition) through Marine Isotope Stages 2 and 3 have not been taken into account in our modeling study.

5. Conclusions

[32] Our study suggests a close relation between AMOC, North Atlantic sea surface temperature and Sahel precipitation. Predictions of the future rainfall in the Sahel are highly uncertain and range from wetter conditions to much drier conditions [*Douville et al.*, 2006; *Intergovernmental Panel on Climate Change* (*IPCC*), 2007]. However, climate projections show that the thermohaline overturning will probably slow down in response to anthropogenic-induced warming [*IPCC*, 2007]. From the results of this study, it seems likely that the future of precipitation in the Sahel will strongly depend on the behavior of the AMOC and its influence on the spatial structure of global warming.

[33] **Acknowledgments.** Constructive comments by two anonymous referees greatly improved the paper. Thanks to Monika Segl and Birgit Meyer-Schack, Wolfgang Bevern, and Helena Filipsson for help with isotope analyses. AMS ^{14}C datings were done by the staff of the Leibniz-Laboratory for Radiometric Dating and Stable Isotope Research in Kiel. The climate model experiments were performed on the IBM pSeries 690 Supercomputer of the Norddeutscher Verbund für Hoch- und Höchstleistungsrechnen (HLRN). This work was funded through the DFG Research Center/Excellence Cluster "The Ocean in the Earth System."

References

Bonan, G. B., K. W. Oleson, M. Vertenstein, S. Levis, X. Zeng, Y. Dai, R. E. Dickinson, and Z.-L. Yang (2002), The land surface climatology of the community land model coupled to the NCAR community climate model, *J. Clim.*, *15*, 3123–3149, doi:10.1175/1520-0442(2002)015<3123:TLSCOT>2.0.CO;2.

Braconnot, P., et al. (2007), Results of PMIP2 coupled simulations of the mid-Holocene and Last Glacial Maximum — Part 2: Feedbacks with emphasis on the location of the ITCZ and mid- and high latitudes heat budget, *Clim. Past*, *3*, 279–296.

Charney, J. G. (1975), Dynamics of deserts and drought in Sahel, *Q. J. R. Meteorol. Soc.*, *101*, 193–202, doi:10.1002/qj.49710142802

Chiang, J. C. H., and A. Koutavas (2004), Climate change — Tropical flip-flop connections, *Nature*, *432*, 684–685, doi:10.1038/432684a.

Citeau, J., L. Finaud, J. P. Cammas, and H. Demarcq (1989), Questions relative to ITCZ migrations over the tropical Atlantic Ocean, sea surface temperature and Senegal River runoff, *Meteorol. Atmos. Phys.*, *41*, 181–190, doi:10.1007/BF01026109.

Cook, K. H., and E. K. Vizy (2006), Coupled model simulations of the West African monsoon system: Twentieth- and twenty-first-century simulations, *J. Clim.*, *19*, 3681–3703, doi:10.1175/JCLI3814.1.

Dahl, K., A. J. Broccoli, and R. J. Stouffer (2005), Assessing the role of North Atlantic freshwater forcing in millennial scale climate variability: A tropical Atlantic perspective, *Clim. Dyn.*, *24*, 325–346, doi:10.1007/s00382-004-0499-5.

de Abreu, L., N. J. Shackleton, J. Schönfeld, M. Hall, and M. Chapman (2003), Millennial-scale oceanic climate variability off the Western Iberian margin during the last two glacial periods, *Mar. Geol.*, *196*, 1–20, doi:10.1016/S0025-3227(03)00046-X.

deMenocal, P. B. (1995), Plio-Pleistocene African climate, *Science*, *270*, 53–59, doi:10.1126/science.270.5233.53.

Douville, H., D. Salas-Mélia, and S. Tyteca (2006), On the tropical origin of uncertainties in the global land precipitation response to global warming, *Clim. Dyn.*, *26*, 367–385, doi:10.1007/s00382-005-0088-2.

Dupont, L. M., H. Behling, and J.-H. Kim (2008), Thirty thousand years of vegetation development and climate change in Angola (Ocean Drilling Program Site 1078), *Clim. Past*, *4*, 111–147.

European Programme for Ice Coring in Antarctica (EPICA) (2006), One-to-one coupling of glacial climate variability in Greenland and Antarctica, *Nature*, *444*, 195–198, doi:10.1038/nature05301.

Fairbanks, R. G., R. A. Mortlock, T.-C. Chiu, L. Cao, A. Kaplan, T. P. Guilderson, T. W. Fairbanks, A. L. Bloom, P. M. Grootes, and M.-J. Nadeau (2005), Radiocarbon calibration curve spanning 0 to 50000 years BP based on paired ^{230}Th/^{234}U/^{238}U and ^{14}C dates on pristine corals, *Quat. Sci. Rev.*, *24*, 1781–1796, doi:10.1016/j.quascirev.2005.04.007.

Folland, C. K., T. N. Palmer, and D. E. Parker (1986), Sahel rainfall and worldwide sea temperatures, 1901–85, *Nature*, *320*, 602–607, doi:10.1038/320602a0.

Gac, J. Y., and A. Kane (1986), Le fleuve Sénégal: I. Bilan hydrologique et flux continentaux de matières particulaires à l'embouchure, *Sci. Geol. Bull.*, *39*, 99–130.

Gasse, F. (2000), Hydrological changes in the African tropics since the Last Glacial Maximum, *Quat. Sci. Rev.*, *19*, 189–211, doi:10.1016/S0277-3791(99)00061-X.

Gasse, F., and E. van Campo (1994), Abrupt post-glacial climate events in West Asia and North Africa monsoon domains, *Earth Planet. Sci. Lett.*, *126*, 435–456, doi:10.1016/0012-821X(94)90123-6.

Govindaraju, K. (1994), 1994 compilation of working values and descriptions for 383 geostandards, *Geostand. Newsl.*, *18*, 1–158.

Grousset, F. E., M. Parra, A. Bory, P. Martinez, P. Bertrand, G. Shimmield, and R. M. Ellam (1998), Saharan wind regimes traced by the Sr-Nd isotopic composition of subtropical Atlantic sediments: Last Glacial Maximum vs today, *Quat. Sci. Rev.*, *17*, 395–409, doi:10.1016/S0277-3791(97)00048-6.

Hales, K., J. D. Neelin, and N. Zeng (2006), Interaction of vegetation and atmospheric dynamical mechanisms in the mid-Holocene African monsoon, *J. Clim.*, *19*, 4105–4120, doi:10.1175/JCLI3833.1.

Intergovernmental Panel on Climate Change (IPCC) (2007), *Climate Change 2007: The Physical Science Basis: Contribution of Working Group I to the Fourth Assessment Report of the Intergovernmental Panel on Climate Change*, edited by S. Solomon et al., 996 pp., Cambridge Univ. Press, New York.

Jullien, E., F. Grousset, B. Malaizé, J. Duprat, M. F. Sanchez-Goni, F. Eynaud, K. Charlier, R. Schneider, A. Bory, V. Bout, and J. A. Flores (2007), Low-latitude "dusty events" vs. high-latitude "icy Heinrich events", *Quat. Res.*, *68*, 379–386, doi:10.1016/j.yqres.2007.07.007.

Kalnay, E., et al. (1996), The NCEP/NCAR 40-year reanalysis project, *Bull. Am. Meteorol. Soc.*, *77*, 437–471, doi:10.1175/1520-0477(1996)077<0437:TNYRP>2.0.CO;2.

Kattan, Z., J. Y. Gac, and J. L. Probst (1987), Suspended sediment load and mechanical erosion in the Senegal Basin — Estimation of the surface runoff concentration and relative contributions of channel and slope erosion, *J. Hydrol. Amsterdam*, *92*, 59–76, doi:10.1016/0022-1694(87)90089-8.

Koopmann, B. (1981), Sedimentation von Saharastaub im subtropischen Nordatlantik während der letzten 25.000 Jahre, *Meteor Forschungsergeb., Reihe C*, *35*, 23–59.

Kröpelin, S., et al. (2008), Climate-driven ecosystem succession in the Sahara: The past 6000 years, *Science*, *320*, 765–768, doi:10.1126/science.1154913.

Lamb, P. J. (1978), Large-scale tropical Atlantic surface circulation patterns associated with sub-Saharan weather anomalies, *Tellus*, *30*, 240–251.

Legates, D. R., and C. J. Willmott (1990), Mean seasonal and spatial variability in gauge-corrected global precipitation, *Int. J. Climatol.*, *10*, 111–127, doi:10.1002/joc.3370100202.

Levis, S., G. B. Bonan, and C. Bonfils (2004), Soil feedback drives the mid-Holocene North African monsoon northward in fully coupled CCSM2 simulations with a dynamic vegetation model, *Clim. Dyn.*, *23*, 791–802, doi:10.1007/s00382-004-0477-y.

Liu, Z., et al. (2007), Simulating the transient evolution and abrupt change of Northern Africa atmosphere-ocean-terrestrial ecosystem in the Holocene, *Quat. Sci. Rev.*, *26*, 1818–1837, doi:10.1016/j.quascirev.2007.03.002.

Liu, Z. Y., Y. Wang, R. Gallimore, M. Notaro, and I. C. Prentice (2006), On the cause of abrupt vegetation collapse in North Africa during the Holocene: Climate variability vs. vegetation feedback, *Geophys. Res. Lett.*, *33*, L22709, doi:10.1029/2006GL028062.

McManus, J. F., R. Francois, J.-M. Gherardi, L. D. Keigwin, and S. Brown-Leger (2004), Collapse and rapid resumption of Atlantic meridional circulation linked to deglacial climate changes, *Nature*, *428*, 834–837, doi:10.1038/nature02494.

Michel, P. (1973), Les bassins des fleuves Sénégal et Gambie, in Étude Géomorphologique, rep., Inst. de Rech. pour le Dév., Paris.

Moreno, T., X. Querol, S. Castillo, A. Alastuey, E. Cuevas, L. Herrmann, M. Mounkaila, J. Elvira, and W. Gibbons (2006), Geochemical variations in aeolian mineral particles from the Sahara-Sahel Dust Corridor, *Chemosphere*, *65*, 261–270, doi:10.1016/j.chemosphere.2006.02.052.

Mulitza, S., and C. Rühlemann (2000), African monsoonal precipitation modulated by interhemispheric temperature gradients, *Quat. Res.*, *53*, 270–274, doi:10.1006/qres.1999.2110.

Newell, R. E., and J. Hsiung (1987), Factors controlling free air and ocean temperature of the last 30 years and extrapolation to the past, in *Abrupt Climatic Change: Evidence and Implications*, edited by W. H. Berger and L. D. Labeyrie, pp. 67–87, Springer, New York.

Nicholson, S. E. (2000), The nature of rainfall variability over Africa on timescales of decades to millenia, *Global Planet. Change*, *26*, 137–158, doi:10.1016/S0921-8181(00)00040-0.

Nicholson, S. E., and J. P. Grist (2003), The seasonal evolution of the atmospheric circulation over West Africa and equatorial Africa, *J. Clim.*, *16*, 1013–1030, doi:10.1175/1520-0442(2003)016<1013:TSEOTA>2.0.CO;2.

Oleson, K. W., et al. (2004), Technical description of the Community Land Model (CLM), *NCAR/TN-461+STR*, 174 pp., Natl. Cent. for Atmos. Res., Boulder, Colo.

Orange, D., J. Y. Gac, and M. I. Diallo (1993), Geochemical assessment of atmospheric deposition including Harmattan dust in continental West Africa, in *Tracers in Hydrology*, edited by N. E. Peters et al., *IAHS Publ.*, *215*, 303–312.

Peck, J. A., R. R. Green, T. Shanahan, J. W. King, J. T. Overpeck, and C. A. Scholz (2004), A magnetic mineral record of Late Quaternary tropical climate variability from Lake Bosumtwi, Ghana, *Palaeogeogr. Palaeoclimatol. Palaeoecol.*, *215*, 37–57.

Prange, M. (2008), The low-resolution CCSM2 revisited: New adjustments and a present-day control run, *Ocean Sci.*, *4*, 151–181.

Prospero, J. M., and T. N. Carlson (1981), Saharan air outbreaks over the tropical North Atlantic, *Pure Appl. Geophys.*, *119*, 677–691, doi:10.1007/BF00878167.

Prospero, J. M., and P. J. Lamb (2003), African droughts and dust transport to the Caribbean: Climate change implications, *Science*, *302*, 1024–1027, doi:10.1126/science.1089915.

Sarnthein, M., G. Tetzlaff, B. Koopmann, K. Wolter, and U. Pflaumann (1981), Glacial and interglacial wind regimes over the eastern subtropical Atlantic and north-west Africa, *Nature*, *293*, 193–196, doi:10.1038/293193a0.

Sarnthein, M., et al. (2000), Fundamental modes and abrupt changes in North Atlantic circulation and climate over the last 60 ky — Concepts, reconstruction and numerical modeling, in *The Northern North Atlantic: A Changing Environment*, edited by P. Schäfer et al., pp. 365–410, Springer, Berlin.

Schefuß, E., S. Schouten, and R. R. Schneider (2005), Climatic controls on central African hydrology during the past 20,000 years, *Nature*, *437*, 1003–1006, doi:10.1038/nature03945.

Schramm, R., and J. Heckel (1998), Fast analysis of traces and major elements with ED (P)XRF using polarized X-rays: TURBOQUANT, *J. Phys. IV*, *8*, 335–342.

Shackleton, N. J., M. A. Hall, and E. Vincent (2000), Phase relationships between millennial-scale events 64,000–24,000 years ago, *Paleoceanography*, *15*, 565–569, doi:10.1029/2000PA000513.

Shackleton, N. J., R. G. Fairbanks, T.-C. Chiu, and F. Parrenin (2004), Absolute calibration of the Greenland time scale: Implications for Antarctic time scales and for δ^{14}C, *Quat. Sci. Rev.*, *23*, 1513–1522, doi:10.1016/j.quascirev.2004.03.006.

Shanahan, T. M., J. T. Overpeck, C. W. Wheeler, J. W. Beck, J. S. Pigati, M. R. Talbot, C. A. Scholz, J. Peck, and J. W. King (2006), Paleoclimatic variations in West Africa from a record of late Pleistocene and Holocene lake level stands of Lake Bosumtwi, Ghana, *Palaeogeogr. Palaeoclimatol. Palaeoecol.*, *242*, 287–302, doi:10.1016/j.palaeo.2006.06.007.

Street-Perrott, F. A., and R. A. Perrott (1990), Abrupt climate fluctuations in the tropics: The influence of Atlantic Ocean circulation, *Nature*, *343*, 607–612, doi:10.1038/343607a0.

Stuut, J.-B., M. Zabel, V. Ratmeyer, P. Helmke, E. Schefuß, G. Lavik, and R. Schneider (2005), Provenance of present-day eolian dust collected off NW Africa, *J. Geophys. Res.*, *110*, D04202, doi:10.1029/2004JD005161.

Wang, Y., M. Notaro, Z. Liu, R. Gallimore, S. Levis, and J. E. Kutzbach (2008), Detecting vegetation-precipitation feedbacks in mid-Holocene North Africa from two climate models, *Clim. Past*, *4*, 59–67.

Weldeab, S., D. W. Lea, R. R. Schneider, and N. Andersen (2007), 155,000 years of West African monsoon and ocean thermal evolution, *Science*, *316*, 1303–1307, doi:10.1126/science.1140461.

Wien, K., D. Wissmann, M. Kölling, and H. D. Schulz (2005), Fast application of X-ray fluorescence spectrometry aboard ship: How good is the new portable Spectro Xepos analyser?, *Geo Mar. Lett.*, *25*, 248–264, doi:10.1007/s00367-004-0206-x.

Yoshioka, M., N. M. Mahowald, A. J. Conley, W. D. Collins, D. W. Fillmore, C. S. Zender, and D. B. Coleman (2007), Impact of desert dust radiative forcing on Sahel precipitation: Relative importance of dust compared to sea surface temperature variations, vegetation changes, and greenhouse gas warming, *J. Clim.*, *20*, 1445–1467, doi:10.1175/JCLI4056.1.

Zeng, N., J. D. Neelin, K.-M. Lau, and C. J. Tucker (1999), Enhancement of interdecadal climate variability in the Sahel by vegetation interaction, *Science*, *286*, 1537–1540, doi:10.1126/science.286.5444.1537.

A. C. Itambi, S. Mulitza, J. Nizou, M. Prange, M. Schulz, J.-B. Stuut, T. von Dobeneck, G. Wefer, and M. Zabel, MARUM and Department of Geosciences, University of Bremen, Leobener Strasse, D-28359 Bremen, Germany. (smulitza@uni-bremen.de)